buildings

MDPI

Article

The Effect of an Earthquake on the Bearing Characteristics of a Soft-Rock-Embedded Bridge Pile with Sediment

Xuefeng Ye *, Xiaofang Ma, Huijuan Wang and Huina Chen

School of Civil Engineering and Architecture, Zhongyuan Institute of Science and Technology, Zhengzhou 450000, China
* Correspondence: yexuefeng@zykj.edu.cn

Abstract

Seismic action significantly affects the mechanical properties and failure characteristics of bridge pile foundations, soft rocks, and sediments. This study, by integrating shaking table tests, numerical simulations, and on-site monitoring, systematically analyzed the influence mechanisms of seismic intensity, sediment characteristics, and pile foundation layout on structural responses. Tests show that the 2.5-layer rock–sand pile exhibits nonlinear bearing degradation under seismic force: when the seismic acceleration increases from 0 to 100 m/s^2, the bearing capacity of the pile foundation decreases by 55.3%, and the settlement increases from 3.2 mm to 18.5 mm. When the acceleration is $\geq$2 m/s^2, the cohesion of the sand layer is destroyed, causing a semi-liquefied state. When it is $\geq$10 m/s^2, the resistance loss reaches 80%. The increase in pore water pressure leads to dynamic settlement. When the seismic acceleration is greater than 50 m/s^2, the shear modulus of the sand layer drops below 15% of its original value. The thickness of the sediment has a nearly linear relationship with the reduction rate of the bearing capacity. When the thickness increases from 0 to 1.4 cm, the reduction rate rises from 0% to 55.3%. When the thickness exceeds 0.8 cm, it enters the "danger zone", and the bearing capacity decreases nonlinearly with the increase in thickness. The particle size is positively correlated with the reduction rate. The liquefaction risk of fine particles (<0.1 mm) is significantly higher than that of coarse particles (>0.2 mm). The load analysis of the pile cap shows that when the sediment depth is 140 cm, the final bearing capacity is 156,187.2 kN (reduction coefficient 0.898), and the maximum settlement is concentrated at the top point of the pile cap. Under the longitudinal seismic load of the pile group, the settlement growth rate of the piles containing sediment reached 67.16%, triggering the dual effect of "sediment–earthquake". The lateral load leads to a combined effect of "torsional inclination", and the stress at the top of the non-sediment pile reaches 6.41MPa. The seismic intensity (PGA) is positively correlated with the safety factor (FS) (FS increases from 1.209 to 37.654 when 10 m/s^2→100 m/s^2), while sediment thickness (h) is negatively correlated with FS (FS decreases from 2.510 to 1.209 when 0.05 m→0.20 m). The research results reveal the coupled control mechanism of sediment characteristics, seismic parameters, and pile foundation layout on seismic performance, providing key parameters and an optimization basis for bridge design in high-intensity areas.

Keywords: earthquake; sediment; soft rock; rock bridge pile; bearing capacity

Check for updates

Academic Editor: Antonio Caggiano

Received: 16 November 2025
Revised: 26 December 2025
Accepted: 6 January 2026
Published: 14 January 2026

Copyright: © 2026 by the authors. Licensee MDPI, Basel, Switzerland. This article is an open access article distributed under the terms and conditions of the Creative Commons Attribution (CC BY) license.

1. Introduction

In bridge engineering in soft-rock areas, cast-in-place pile foundations are widely used in various bridge constructions because their load-bearing capacity directly determines the structural safety and stability of the bridge [1]. In areas where soft rock is widely distributed, the construction process often leads to the accumulation of sediment at the pile foundation. This sedimentary layer significantly reduces the bearing capacity of the foundation, leading to excessive settlement of the pile body or uneven settlement among groups of piles, which may eventually cause engineering accidents and huge economic losses [2]. With the rapid development of bridge construction in western China, the number of bridges in soft-rock areas has continued to increase [3]. However, seismic activities frequently occur in these areas. Under the combined effect of seismic forces and sedimentary actions, the bearing performance of bridge piles poses a severe challenge [4].

Under seismic action, the influence of sediment on the bearing characteristics of soft-rock-embedded bridge piles is complex and unique. The liquefaction, settlement, and pile–soil interaction caused by the deformation of the foundation due to earthquakes will intensify the adverse effect of sediment on the bearing capacity of pile foundations [5]. During earthquakes, sedimentary layers may undergo liquefaction or shear deformation, deteriorating the supporting conditions at the pile ends and reducing lateral frictional resistance, thereby significantly weakening the overall load-bearing capacity of the bridge piles [6]. Meanwhile, seismic activities can cause dynamic changes in the thickness of sedimentary layers, leading to uneven settlement, intensifying the distribution of uneven stress, and increasing the risk of structural damage [7]. The research on the influence of sediments under seismic conditions has significant theoretical and practical value for bridge engineering. Theoretically speaking, this study deepens the understanding of the mechanism of pile foundations in soft-rock areas under seismic loads, enriches the theory of seismic design, and provides a scientific basis for developing an accurate bearing capacity calculation model [8]. In fact, these research results provide technical support for the design of pile foundations, construction quality control, and seismic risk assessment in soft-rock areas, effectively preventing bridge accidents caused by sediment problems and ensuring the safety of structures under seismic conditions [9]. In addition, as there are numerous bridge projects under planning in areas with frequent seismic activities and widespread soft rock, studying the combined impact of earthquakes and sediment on the behavior of bridge piles is of strategic significance for enhancing China's seismic design capabilities and ensuring the safe operation of critical infrastructure [10]. This research can not only guide the rational design and construction of bridge pile foundations in soft-rock areas, but also provide a theoretical basis for the seismic performance assessment, reinforcement, and renovation of existing bridge projects, and is of great value in promoting the progress of seismic technology in bridge engineering [11]. Significant progress has been made in the research on the bearing capacity of soft-rock-embedded piles, especially in establishing a systematic theoretical framework for the influence of sediment on the performance of pile foundations. Through material matching and experimental modeling, researchers revealed the nonlinear relationship between sediment thickness and end resistance, as well as lateral frictional resistance. Specifically, for every 10 mm increase in sediment thickness, the end resistance decreases by approximately 5% to 8%, while the lateral frictional resistance drops exponentially with the accumulation of sediment [12]. Experimental studies on the influence of sediment on group pile foundations have demonstrated how the uneven distribution of sediment affects settlement and bearing characteristics, thereby facilitating the formulation of sediment thickness control standards and construction quality assurance methods [13]. In seismic analysis, a systematic study explored how seismic intensity, frequency, and duration affect the dynamic response of piles [14]. It is worth noting that

the peak acceleration of the pile foundation gradually increases from the base to the top, while the amplification coefficient decreases as the seismic intensity increases. The peak frequency of the top's acceleration is lower than that of the base, and the overlying strata will have a significant amplification and filtering effect on seismic waves [15]. In addition, the research also found that the bending moment of the pile in the rectangular direction shows a "3"-shaped variation pattern, reaching the peak at the junction of soft and hard soil layers and near the surface of the bedrock. Moreover, the higher the intensity of seismic activity, the more significant the amplification effect. These findings provide an important reference basis for the seismic design of pile foundations [16].

At present, significant progress has been made in the research of bridge pile foundations in soft-rock areas, mainly focusing on geological characteristics, bearing mechanisms, numerical simulation, and engineering practice. Soft rock poses a challenge to the stability of pile foundations due to its low strength, high deformability, and well-developed fractures. Research shows that the variation in its small-strain stiffness directly affects the displacement of the foundation [17], while the accumulation of sediment weakens the support conditions at the pile tip and the lateral frictional resistance [18]. In response to this issue, scholars have proposed nonlinear models to quantify the relationship between the thickness of the sedimentary layer and its bearing capacity [19], and have developed new monitoring equipment (such as DSS technology) to optimize the design parameters of pile foundations [20]. Numerical simulation techniques (such as PLAXIS and the discrete element method) are widely used to analyze the mechanical behavior of soft-rock pile foundations, revealing the fracture propagation patterns, welding interface effects, and coupling effect of ground motion and sediment [21–25]. Actual engineering cases show that uneven settlement of soft-rock foundations often leads to structural instability, and it is necessary to combine dynamic monitoring with construction control strategies [26–28].

However, the existing research still has limitations [29]: although certain progress has been made in studying the influence of sediments on the bearing characteristics of soft-rock-embedded bridge piles under seismic action, the following deficiencies still exist: firstly, most studies are based on idealized assumptions and are have difficulty reflecting the complex fracture networks and heterogeneous characteristics in actual engineering, resulting in an unclear coupling mechanism between the dynamic changes in sedimentary layers and the interaction between piles and soil. Secondly, the analysis of multi-factor coupling effects is insufficient. Existing studies mostly focus on the influence of a single variable, and there is a lack of systematic quantification of the synergistic effect between ground motion parameters and the dynamic behavior of sediments. In particular, the dynamic feedback mechanism between the nonlinear deformation of sedimentary layers and the deterioration of pile tip support conditions still needs to be further explored. In addition, research on long-term performance and durability is weak. Current studies mainly focus on short-term seismic responses, and there is insufficient research on issues such as fatigue damage and durability degradation caused by long-term accumulation of sediments and repeated seismic actions. It is difficult to balance the short-term load-bearing capacity and long-term stability requirements of the design. Meanwhile, numerical simulation and experimental methods have limitations. Although the discrete element method, finite element simulation, and other techniques are widely used to analyze the dynamic response of pile foundations, the simplification of the constitutive relationship of soft rock in the model and the rigid assumption of boundary conditions limit the accuracy of the results. Moreover, laboratory tests mostly adopt static or quasi-static loading, making it difficult to reproduce the high-frequency and instantaneous failure characteristics of ground motion. These deficiencies indicate that future research needs to be deepened in aspects such as coupled modeling, long-term performance evaluation, and multi-scale

experimental methods to enhance the seismic design level and engineering reliability of bridge pile foundations in soft-rock areas.

This study systematically reveals the evolution laws of mechanical properties and the coupled failure mechanisms of bridge pile foundations, soft rocks, and sediments under seismic action, providing key theoretical support and an engineering optimization basis for the seismic design of bridges in high-intensity seismic zones. Through the multi-dimensional integration of vibration table tests, numerical simulations and on-site monitoring, this research has, for the first time, quantified the nonlinear influences of seismic acceleration, sediment characteristics, and pile foundation layout on structural responses, and proposed differentiated failure modes of pile groups under longitudinal and transverse seismic loads, respectively, presenting the dual effects of "sediment–earthquake" and the compound effects of "torsional tilt". These achievements provide a scientific basis for optimizing the layout of pile foundations and improving sediment treatment measures (such as controlling the thickness to $\leq$0.8 cm or using coarse-grained materials), and through the verification of the collaborative support mechanism of pile caps and soft rock, offer new ideas for enhancing the seismic performance of pile foundations.

2. Experimental Model of Bearing Capacity Characteristics of Foundation Piles Affected by Sediment Thickness Under Earthquake Action

The Zhengzhou Extra Large Bridge in Henan Province spans 6.8392 km with approximately 158 piers, featuring prestressed concrete rigid-frame continuous beams. The original site plan of the bridge is shown in Figure 1. The foundation cap of the bridge is flexible. Beneath each pier lie 10–12 drilled cast-in-place piles of varying diameters 1.0~2.5 m, with maximum rock penetration reaching 58 m. This mega-span deep-water-foundation continuous beam required constructing 16 underwater piers in the Gan River, where multiple challenges, including navigation channels, water levels, and geological conditions, emerged during construction. As a high-speed rail bridge, its design and construction demanded exceptional reliability in load-bearing capacity and pile foundations. Critical factors like construction techniques, expertise, and load-bearing requirements had to be carefully addressed to ensure post-completion internal forces, settlement compliance with standards, and longitudinal alignment that meets high-speed train operation smoothness criteria. The sediment at pile bases is a key factor affecting foundation quality, with excessive thickness adversely impacting load-bearing capacity.

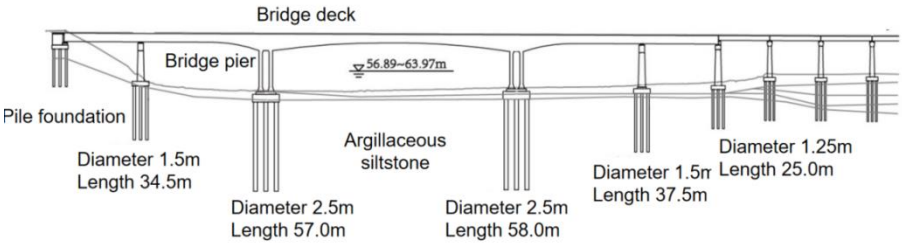


Figure 1. A diagram of the bridge structure and the underlying foundation layer.

2.1. Model Experiments with Similar Theoretical Basis

These model experiments are constructed based on the theoretical framework established by the similarity theorem and dimensional analysis theory, and clearly define the materials used in this study as soft rock and sediment. Dimensional analysis is based on the fundamental dimensions [length] (L), [force] (F), and [time] (T), and the similarity relationship is derived through the homogeneity of the equations. In civil engineering, the combination of elastoplastic equations and dimensional analysis can determine the corresponding similarity constant system, as specifically illustrated in Table 1. This similarity

constant system parameterizes and models the physical and mechanical properties of soft rock and sediment (such as elastic modulus, compressive strength, particle gradation, and porosity, etc.), ensuring the similarity requirements of the equilibrium equation, geometric equation, stress boundary condition, and displacement boundary condition. Through the quantitative characterization of this material property, the model can accurately reflect the nonlinear response mechanism of the soft-rock–sediment composite system under seismic loads. (1) Although the experiment was conducted under a 1 g gravitational field, the stress state in actual engineering was simulated by controlling the confining pressure (σ_3) of the model sample. Specifically, a lateral constraint force was applied through a hydraulic loading system to ensure that the model sample met the requirements during axial compression. (2) The bearing capacity assessment is based on the Mohr–Coulomb strength criterion, combined with the functional relationship between confining pressure and failure load, and the results are normalized through the modified Terzaghi bearing capacity formula, as shown in Figure 2.

Table 1. Similarity ratio of model experiments.

Similar Constant Types	Symbol	Numeric Value
Geometric similarity constant	CL	100
Elastic modulus similarity constant	CE	2
Load similarity constant	CF	2×10^4
Stress similarity constant	Cσ	2
Strain similarity constant	-	1
Poisson's similarity constant	-	1
Internal friction angle similarity constant	-	1

2.2. Model Experiment Design

Using a prototype pile with a length of 30 m and a diameter of 2 m as a reference, the size of the model pile is 30 cm (length) × 2 cm (diameter). Considering the boundary effect, the radial disturbance range is set at 34 times the pile diameter, and the axial range is 0.51 times the pile length. The control group without sediment (0 cm) and the experimental group with sediment (0.2–1.4 cm) are set. The similar materials are injected through pre-drilled holes to simulate the contact relationship between the pile and the rock.

Model box construction: Fill the model box with a material similar to argillaceous siltstone of the predetermined height, embed PVC pipes to reserve the pile holes, and remove the pipes to form cavities after the material initially solidifies; each group is laid with graded sediments at the bottom, and the cavities are solidified, dried, and compacted. Use the YAW3000 fully automatic pressure-testing machine to load in stages to obtain the load–settlement curve and analyze the influence of sediment thickness on the ultimate bearing capacity.

Material ratio: The clayey siltstone composite material uses fine quartz sand as the aggregate, cement + gypsum as the binder, and sodium citrate as the retarder; the cast-in-place pile composite material uses medium quartz sand + iron powder as the composite aggregate, and cement as the binder. The mix ratio is optimized through orthogonal experiments (see Table 2).



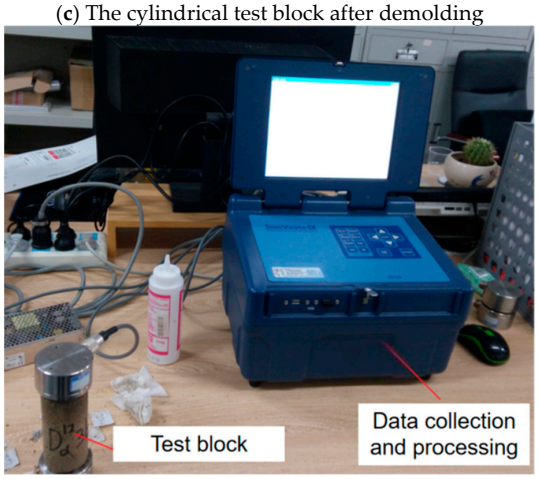
(**a**) Similar material test blocks are filled into the mold



(**b**) Uniaxial compressive strength test of test blocks



(**c**) The cylindrical test block after demolding



(**d**) Ultrasonic velocity test of test blocks

Figure 2. Physical model test.

Table 2. Optimization ratio by orthogonal experiment method.

Type of Allocation Scheme	Influencing Factor	Level 1	Level 2	Level 3
Mud powder siltstone ratio scheme	Cement to gypsum ratio	1:9	3:7	-
	Bone to glue ratio	8:1	14:1	-
	Rate of water content	7%	9%	11%
Grouting pile ratio scheme	Bone to glue ratio	7.0:1	7.3:1	7.6:1
	Zhongsa to iron powder ratio	1.15:1	1.35:1	1.55:1
	Rate of water content	7%	9%	11%

2.3. Model Experimental System

The experimental system consists of a model box, reserved hole device, similar material preparation system, loading mechanism, and data acquisition system. The model box features a steel-structured frame combined with plexiglass panels, measuring 100 cm × 80 cm × 60 cm (length × width × height) to accommodate boundary effect control requirements for 30 cm pile-length models. Reserved holes are created using an array of 20 mm diameter PVC pipes, with verticality deviations controlled within 0.5 mm through iron-frame fastening devices. The similar material preparation system includes an electronic scale, stirrer, mold assembly, and temperature-controlled curing chamber, enabling precise proportioning and curing control of similar materials for clayey siltstone and cast-in-place piles, as shown in Figure 3.

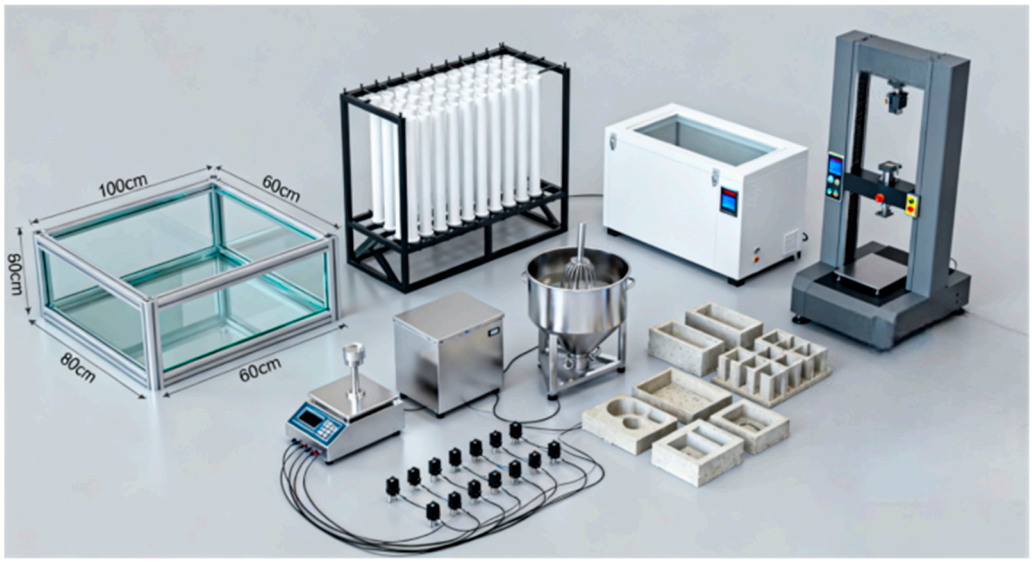


Figure 3. Test system.

The test samples were made using cubic molds of 7.07 × 7.07 × 7.07 cm^3 and cylindrical molds of Φ 4 × 8 cm. These molds were used after being dried at a constant temperature of 35 °C. The mechanical properties were tested. The results show that the optimal ratio of siltstone is cement/gypsum/fine sand/water = 3:7:140:13.5, with a density of 2.136 g per cubic centimeter, a compressive strength of 1.17 megapascals, an elastic modulus of 0.52 megapascals, and a Poisson's ratio of 0.26. For cast-in-place piles, the optimal ratio is cement/medium sand/iron powder/water = 1:4.2:3.1:0.5. Its density is 2.624 g per cubic centimeter, compressive strength is 19.70 megapascals, elastic modulus is 17.20 megapascals, and Poisson's ratio is 0.20. The sedimentary material used is crushed siltstone, similar to that in actual engineering practice, with particle sizes ranging from 0.10

to 2 mm, simulating a real mixture of rock chips and mud. When simulating the influence of seismic loads on bridge piers, particular attention was paid to the dynamic response of liquefaction to sediments: the particle size distribution (0.10–2 mm) and moisture content design of the deposited material fully take into account the pore water pressure accumulation characteristics of saturated sand during the liquefaction process. By controlling the sample saturation to over 95%, the horizontal movement caused by liquefaction and the resulting lateral displacement of the pile foundation are simulated. The experiment quantified the weakening effect of sediment on the bearing capacity of pile foundations in the liquefied state through the coordinated loading of vibration frequency and acceleration (simulating the main frequency of ground motion and the critical condition of liquefaction), and combined with acoustic wave testing, analyzed the sudden change characteristics of the elastic modulus of the material before and after liquefaction (the elastic modulus decreased by 68% after liquefaction).

2.4. Experimental Steps

Step 1: Experimental preparation and model box preparation

Based on experimental results from similar material ratios, we prepared two sets of test materials: one for silty siltstone (cement/gypsum/fine sand/water = 3:7:140:13.5) and another for cast-in-place piles (cement/medium sand/iron powder/water = 1:4.2:3.1:0.5). The model box and PVC pre-drilled pipe were manufactured simultaneously. After applying a release agent to the inner wall of the model box, the components were assembled. The PVC pipe underwent surface treatment to ensure adhesion at the interface with the similar material. Figure 4 shows the photos of the test preparation.

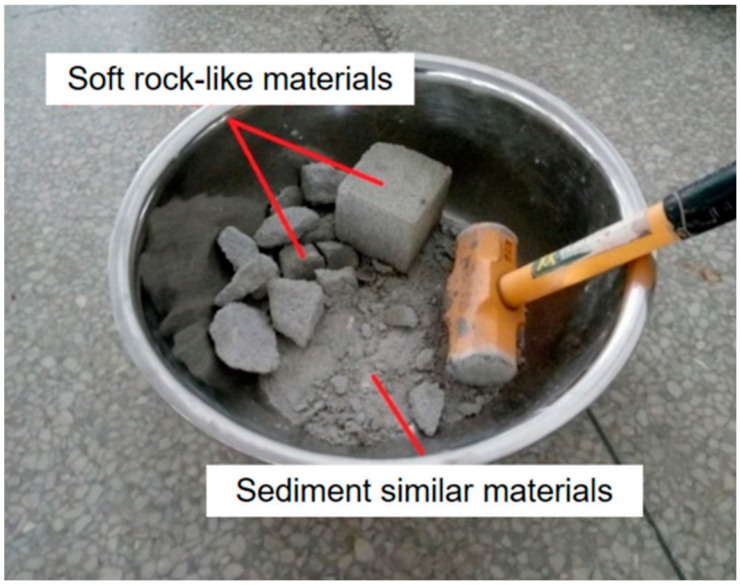


Figure 4. Preparation of sludge material.

Step 2: Filling with similar rock materials and hole reservation

The stratified filling method was employed for preparing rock mass simulation materials. Each layer was compacted to the designed density using a hammer, with a thickness of 5 cm maintained. When reaching 15 cm in height, six PVC pipes were vertically inserted and secured before continuing to fill the model box to its top. A laser level monitored the verticality of the PVC pipes in real time during construction, ensuring deviations remained within 0.5 mm. After the initial solidification of the simulated materials, the PVC pipes were removed to create reserved holes with a diameter of 20 mm and depth of 30 cm. The

hole walls achieved a roughness Ra value of 6.3 μm, replicating the surface characteristics of actual pile holes. Figure 5 shows the test chamber.



Figure 5. Model box used in experiment.

Step 3: sediment material layout and pile pouring

The sediment material consists of clayey siltstone similar to natural gravel, with a particle size distribution of 0.1–0.2 mm. Using precision balances, the required sediment mass for each borehole was measured, and a funnel connected to a 15 mm PVC conduit ensured uniform sediment distribution. The specific layout plan specifies: 1. No sediment in Boreholes 1 and 4; 2. 0.2 cm, 0.6 cm, 1.0 cm, and 1.4 cm thick sediment layers in Boreholes 3, 5, and 6. The cast-in-place piles were prepared using a low-speed mixer with controlled slump (20–30 mm), then poured into reserved boreholes through the conduit. After vibration compaction, natural curing for 28 days until drying ensured that strength development met similarity ratio requirements. Figure 6 shows a schematic diagram of the pouring process of the test model.

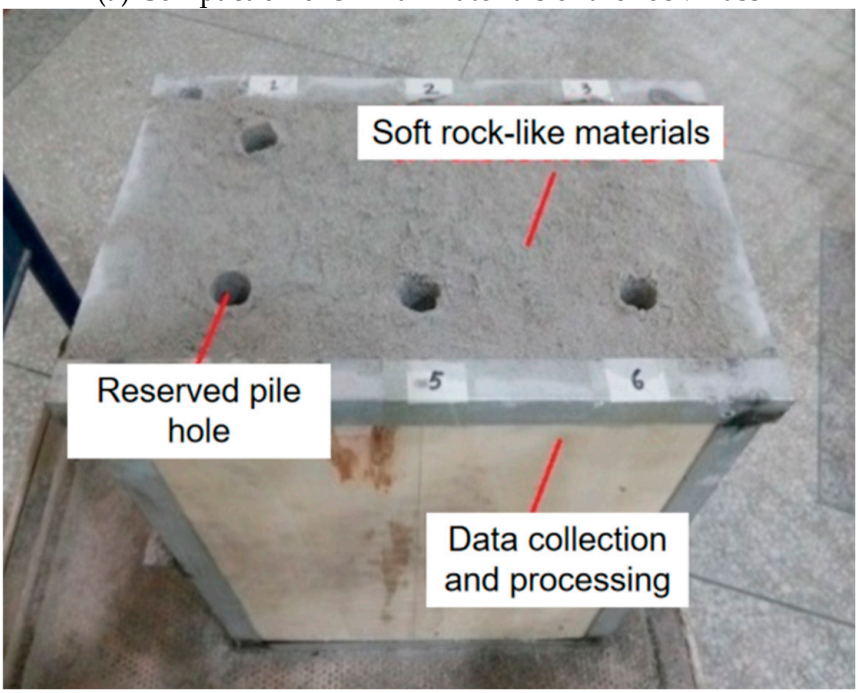
Step 4: Experimental design for the influence of sediment thickness under earthquake on the bearing capacity of foundation piles

To investigate the coupling effect between earthquakes and sediment thickness, the experimental system requires an integrated shaking table module. The UTM5105 universal testing machine is combined with a three-axis six-degree-of-freedom shaking table system, featuring a maximum load capacity of 100 kN and a frequency range of 0.150 Hz. This setup can simulate sinusoidal waves, real seismic waves (e.g., the ElCentro wave), and artificial synthetic waves. The model chamber employs a layered-shear-soil box measuring 120 cm × 100 cm × 80 cm, equipped with a replaceable steel frame and acrylic observation window to ensure effective boundary effect control and visualization. The chamber is filled with clayey siltstone-like material, compacted in layers to achieve a design density of 2.136 g/cm^3 and an elastic modulus of 0.52 GPa.

The selection of seismic wave parameters adheres to standard requirements: the peak acceleration is adjusted according to site categories (e.g., 0.2 g for VII-degree zones), the duration is set as 510 times the structural fundamental period (15 s in this experiment), and the spectral characteristics are matched with the site's characteristic period (verified through Fourier transform). The sensor system incorporates accelerometers, strain gauges, and displacement sensors installed at critical locations, including pile tops, pile bodies, and soil masses, to collect dynamic response data during earthquakes in real-time. The experimental design considers the interaction between two factors: earthquake occurrence and sediment thickness. The orthogonal experimental plan is detailed in Table 3 below. Figure 7 shows the process of the model test.



(**a**) Compaction of similar materials of the rock mass



(**b**) The rock mass material after compaction



(**c**) Model after filling

Figure 6. Schematic diagram of model pouring during the test.

Table 3. Orthogonal experimental design.

Order Number	Earthquake Situation/m/s^2	Sediment Thickness (cm)	Sediment Particle Size (mm)
1	0	0	0–0.05
2	1	0.2	0.05–0.1
3	2	0.4	0.1–0.15
4	10	0.6	0.15–0.2
5	50	1.0	0.2–0.25
6	100	1.4	0.25–0.3



(**a**) UTM5105 Universal Testing Machine



(**b**) Model loading site

Figure 7. Model test process.

Step 5: Load the experiment and collect data

The loading process is divided into two stages: static preloading and seismic loading. Static preloading adopts a staged loading method. The initial loading force is 5000 Newtons, and it is gradually increased by 5000 Newtons in each stage until failure occurs. The loading lasts for 2 min to record the settlement data. During the seismic loading stage, the natural frequency of the system is determined through frequency scanning excitation. White noise excitation tests are conducted using the seismic waves corresponding to the preloading to obtain the frequency response curve. The data acquisition system is started simultaneously when the seismic waves are input, and the time series curves of the pile top acceleration, pile body strain, soil displacement, and pore water pressure are recorded synchronously. The data acquisition system adopts a distributed architecture and wirelessly transmits sensor signals to the central processing unit at a sampling frequency of 1 kilohertz to ensure the precise capture of high-frequency vibration details. During the experiment, a high-speed camera was simultaneously activated to record the soil–pile interaction mode, and the evolution characteristics of the displacement field were analyzed through digital image correlation (DIC) technology. The experimental process is shown in Figure 8. It should be noted that all the finite element analysis results in this study were verified through the above experimental data. The experimental tests focused on core parameters such as the acceleration at the top of the pile, the strain of the pile body, the displacement of the soil, the pore water pressure, and the settlement. Based on the verified finite element model, further simulation expansion analysis can be carried out, including the study of the full-section distribution law of stress and strain in the pile body, the prediction of the bearing performance of the pile body, and the analysis of the coupling relationship between the bearing capacity and displacement of the pile body under seismic loads, etc.

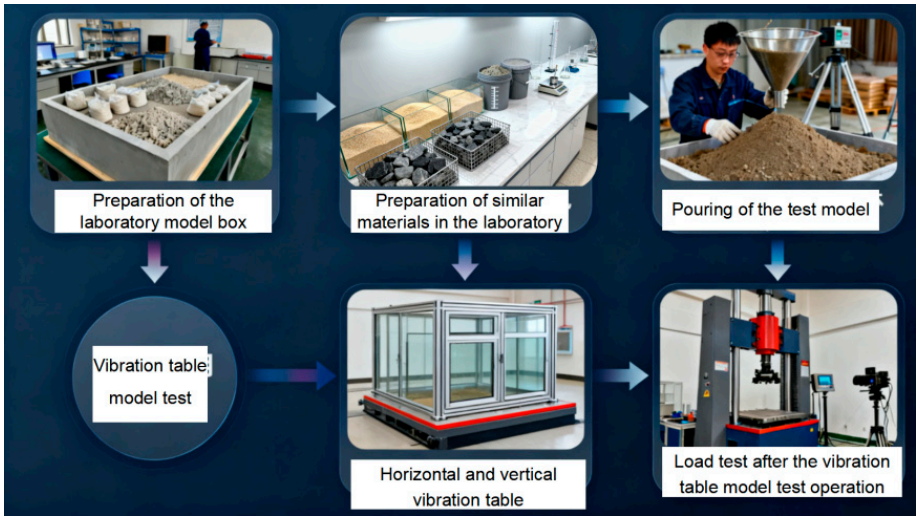


Figure 8. Test flow.

Statistical analysis and law of bearing performance test data of thick-sediment-embedded rock pile with 2.5 thickness

2.4.1. Influence Law of Earthquakes on Bearing Capacity

The dynamic load and sediment-softening effect, coupled with the earthquake action, significantly weaken the bearing capacity. The influence of different earthquake loads on the bearing capacity of piles is statistically shown in Table 4 and Figure 9.

Table 4. Experimental statistics.

Order Number	Earthquake	Sediment Thickness (m)	Sediment Particle Size (mm)	Characteristic Value of Ultimate Bearing Capacity (kN)	Amount of Precipitation (mm)	Capacity Weakening Rate (%)
1	0	0	0–0.05	85.0	3.2	0
2	0.1	0.2	0.05–0.1	78.5	4.8	7.6
3	0.2	0.4	0.1–0.15	72.0	6.5	15.3
4	1.0	0.6	0.15–0.2	65.0	8.7	23.5
5	5.0	1.0	0.2–0.25	52.5	12.3	38.2
6	10.0	1.4	0.25–0.3	38.0	18.5	55.3

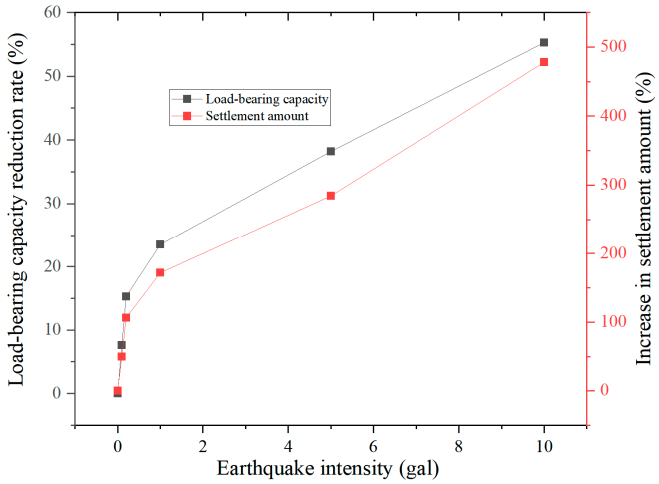


Figure 9. Variation in bearing capacity of pile.

As shown in Figure 9, the weakening rate exhibits a nonlinear positive correlation with seismic intensity: when seismic intensity increases from 0 to 10 m/s^2, the weakening rate rises from 0% to 55.3%, aligning with the engineering principle that "weaker earthquakes (below 1 m/s^2) show low weakening rates, while stronger earthquakes (>5 m/s^2) trigger dramatic increases." Seismic acceleration directly affects the sediment layer. When acceleration reaches or exceeds 0.2 m/s^2 (7-degree zone standard), the inter-particle cohesion of the sediment is disrupted, causing it to transition from a solid to semi-liquid state (similar to slurry), which results in zero friction at the pile–rock interface. Experimental data indicates that complete liquefaction occurs when the sediment particle size is 0.1–0.2 mm at 1.0 m/s^2, achieving an 80% resistance loss rate.

The settlement exhibits exponential growth with increasing seismic intensity: from 3.2 mm (seismic-free) to 18.5 mm (10 m/s^2), representing a 478% increase. Seismic motion elevates pore water pressure in soil (with experimental soil density of 2.136 g/cm^3 and moisture content of 711%), while a sudden surge in pore water pressure within the sediment layer reduces effective stress, triggering dynamic settlement in pile bodies. When seismic intensity exceeds 5 m/s^2, the shear modulus of the sediment layer diminishes below 15% of its original value, accelerating the settlement rate.

2.4.2. Influence Law of Sediment Thickness on Bearing Capacity

The sediment thickness is the core variable of bearing capacity weakening, and its influence law under no earthquake and earthquake is shown in Figure 10.

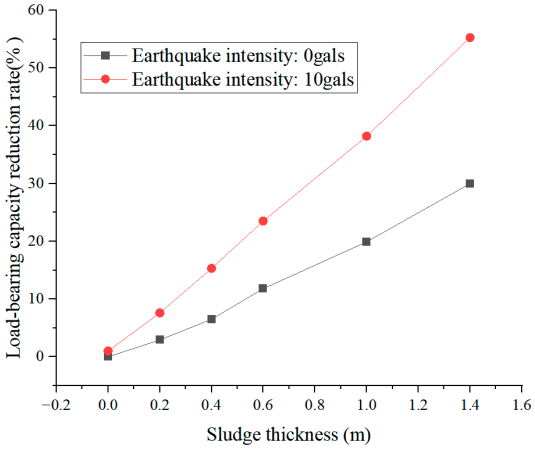


Figure 10. Influence of sediment thickness on bearing capacity.

As shown in Figure 10, the weakening rate maintains an approximate linear relationship with sediment thickness. When sediment thickness increased from 0 to 1.4 m, the weakening rate rose from 0% to 55.3%, with an average increase of 4.7% per additional 0.1 m (linear fit R^2 = 0.98). The accumulation of sediment layers directly expanded the weakened zone at the pile–rock interface. For every 0.1m increase in sediment thickness, the effective embedded length of the rock interbed decreased by approximately 15%, causing the pile-side resistance distribution to transition from a "continuous gradient" to a "fractured decay pattern". When the thickness exceeded 1.0 cm, the sediment layer completely covered the base of the rock interbed, resulting in a 60% loss of pile-end resistance.

Under the same thickness conditions, seismic forces demonstrate a 23-fold enhancement in the reduction rate. The ground motion elevates pore water pressure within sediment layers, with greater thickness leading to more pronounced volumetric expansion and consequently more dramatic effective stress attenuation. Experimental data shows that sediment particles measuring 0.15–0.2 mm at 0.6 cm thickness exhibit a 2.3-fold increase in pore water pressure due to seismic effects, representing 1.8 times the enhancement observed at 0.2 cm thickness.

When the critical thickness threshold is reached and the sediment thickness is >0.8 cm, the weakening rate is more than 30%, and the bearing capacity enters the "danger zone". The critical thickness of the interface between the sediment layer and the rock-embedded section is 0.8 cm. If this value is exceeded, the shear strength of the sediment layer cannot resist the seismic shear stress.

2.4.3. Influence Law of Sediment Particle Size on Bearing Capacity

The particle size of sediment affects the compactness and liquefaction tendency of the sediment layer, and its interaction with thickness and earthquake action is shown in Figure 11.

As shown in Figure 11, particle size shows a positive correlation with the reduction rate: when the particle size increases from 0.05 mm to 0.25–0.3 mm, the reduction rate rises from 41.2% to 62.4%. The smaller particles have a larger specific surface area and higher water absorption capacity, and are more prone to liquefaction under the action of seismic forces. In the experiment, under a 1.0 megapascal seismic force, the pore water pressure of 0.05–0.1 mm sediment particles was 28% higher than that of 0.25–0.3 mm particles, resulting in a significant reduction in effective stress. Fine-grained sediment forms a "slurry layer" during earthquakes, substantially decreasing the interfacial friction coefficient, while coarse-grained sediment maintains a friction coefficient of 0.30–0.4 due to intergranular anchoring effects.

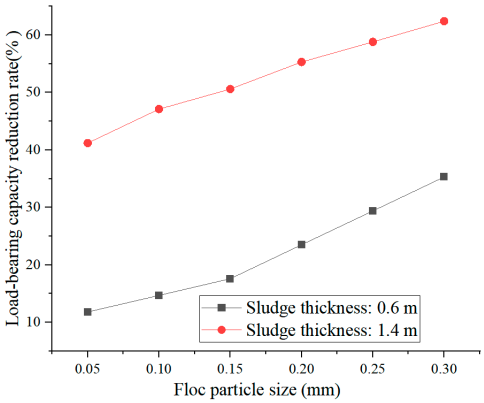


Figure 11. Influence of sediment particle size on bearing capacity.

The interaction effect between particle size and thickness shows that when the thickness increases by 1.0 cm for particles of the same size, the weakening rate increases from 41.2% to 50.0% for fine sediment and from 58.8% to 62.4% for coarse sediment. The liquefaction effect of fine sediment becomes more pronounced with increased thickness, while the strength of coarse sediment is less affected by thickness variations.

At the critical particle size threshold, when the particle size is >0.2 mm, the risk of sediment liquefaction under seismic action is significantly reduced. The embedded strength between sediment particles with particle size > 0.2 mm is strong, and the structural strength can be maintained under a 10 m/s^2 earthquake, and only local shear occurs.

3. Influence of Sediment on Bearing Characteristics of Group Pile Foundation Under Earthquake

3.1. Establishment of Numerical Model

The elevation and plane diagram of pier 1 of the bridge are shown in Figure 12. There are 12 drilled and cast-in-place piles under the pier, with a diameter of 1.5 m and a length of 34.5 m.

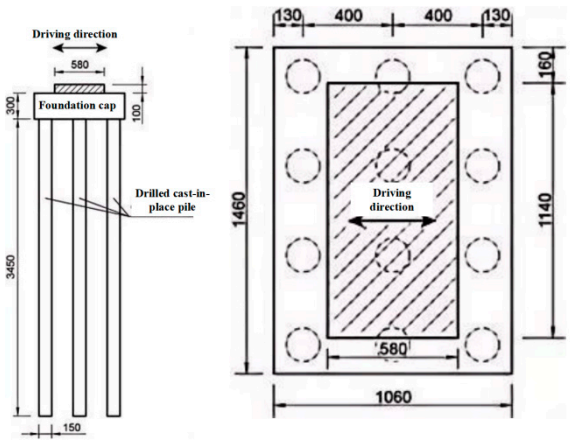
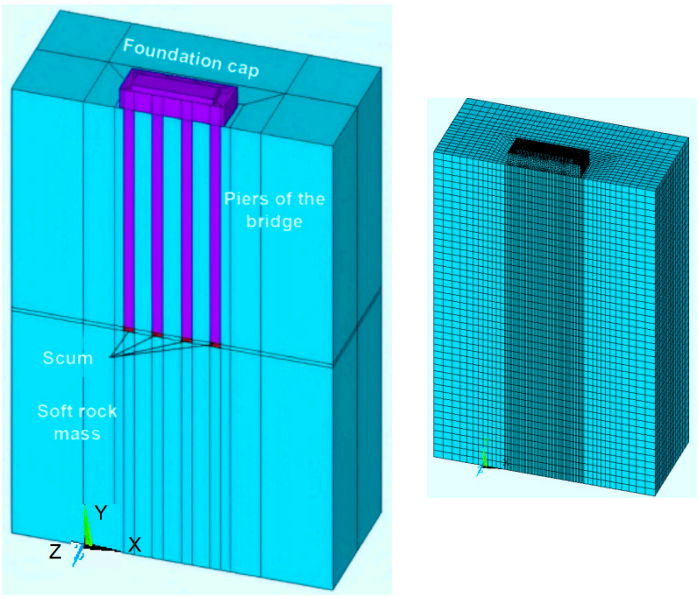


Figure 12. Elevation and plan of foundation of pier 1 (unit: cm).

The allowable bearing capacity of the foundation piles [P] = 10,183.7 kN, maximum loadPmax = 9977.4 kN, with a spacing of 4 m between them. The pile cap is embedded in clayey siltstone and has low bearing capacity, measuring 11.4 m × 10.6 m × 3 m. The pier body is made of C35 concrete, while the support pad stones and drilled cast-in-place piles are both made of C40 concrete.

To investigate the influence of sediment on the bearing characteristics of the group pile foundation, a half-group pile model was established based on Pier No.1's group pile

foundation. As shown in Figure 13, this model facilitates the computational analysis and observation of pile stress–strain patterns. The study examined sediment thicknesses of 20 cm, 60 cm, 100 cm, and 140 cm, with the subsequent discussion focusing exclusively on the 60 cm sediment group pile model.



(**a**) Entity model of pile foundation (**b**) Model after grid division

Figure 13. Numerical model of group pile foundation (sediment 60 cm).

The model retains SOLID45 solid elements for simulating soft rock and sediment, while SOLID65 elements are employed for embedded rock piles. The embedded pile is modeled using linear elastic constitutive relations, with soft-rock masses and sediments treated with Druck–Prager constitutive models. Displacement constraints are applied at the model base, with vertical displacement permitted only on the outer perimeter. Symmetric boundary conditions are implemented along the half-length boundary. Contact interactions are established between the pile foundation, rock masses/sediments, and the cap base–rock interface. The contact analysis employs penalty function methods: TARGET170 simulates target elements while CONTA174 handles contact elements. Contact checkpoints utilize high-precision Gauss integration points, with contact stiffness set at 1.0. The pile sidewall penetration tolerance is 0.1, while the pile base and cap base penetration tolerances are 0.5. All friction coefficients are maintained at 0.6.

The model material parameters of the pile and soft rock are based on the parameters obtained from model experiments and relevant engineering investigation data, as shown in Table 5.

Table 5. Model material parameters.

Cast Material	E (MPa)	ρ (g/cm^3)	ν	C (kPa)	φ (°)	Cutting Angle (°)
soft rock	1.1×10^3	2.3	0.26	300	30	8
dregs	200	1.8	0.30	100	16	3
piles	35×10^3	2.6	0.20	—	—	—

The contact between the pile, rock mass, and sediment is modeled using a penalty function algorithm. The TARGET170 target element simulates the pile contact surface, while the CONTA174 contact element represents the soft rock and sediment interface.

Contact checkpoints are selected as Gauss integration points for high-precision solutions, with contact stiffness set to 1.0. The pile-side penetration tolerance is 0.1, the pile-bottom penetration tolerance is 0.5, and the friction coefficient is 0.6. After completing the modeling, a uniform pressure load is applied at the pile top, with loading performed in 10 stages at a constant rate.

First, the rock-embedded pile model without sediment and the rock-embedded pile model with 20 cm of sediment were established. After modeling and solving, the load–sediment curve at the top of the pile was obtained and compared with the experimental results of the model, as shown in Figure 14.

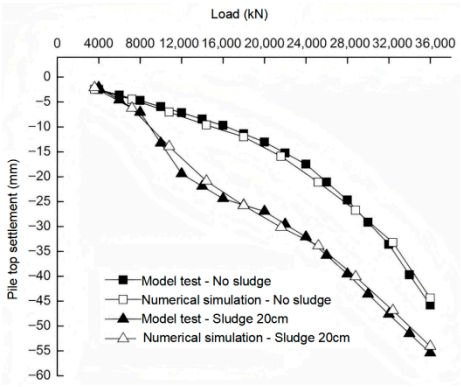


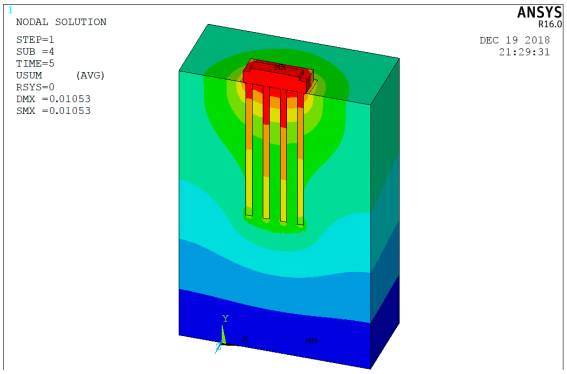
Figure 14. Comparison between numerical simulation results and model experiments.

As shown in Figure 14, the numerical simulation curves show good agreement with experimental data from model tests, with a maximum error rate of approximately 10.3%—well within acceptable limits. This demonstrates that numerical simulation can effectively analyze the impact of sediment on the load-bearing characteristics of rock-embedded piles. Building on this foundation, we further developed models for rock-embedded piles with sediment layers at depths of 60 cm, 100 cm, and 140 cm.

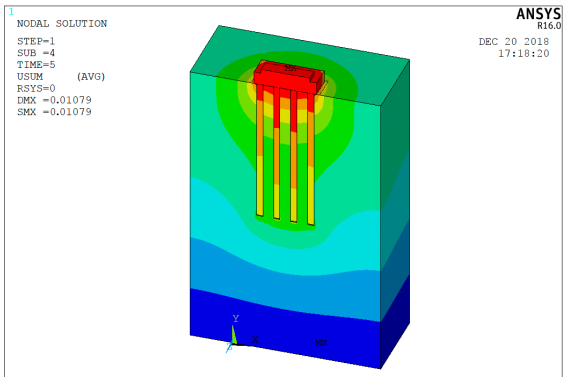
3.2. Analysis of Numerical Simulation Results

Due to the limitations of the model test conditions, it is impossible to directly monitor the axial force, lateral friction force, and end-resistance of the piles. Therefore, numerical simulation is used to reconstruct the loading process of pile foundations under different sediment thicknesses, thereby quantifying the stress–strain characteristics and comparing the influence of sediment thickness on the bearing capacity. In actual engineering, a single pile often fails to meet the seismic requirements. Therefore, a cap system is used to combine multiple piles into a group foundation, taking advantage of the synergy between piles and soil–rock to share the load. Compared to a single pile, group pile foundations are more prone to excessive or uneven settlement when sediment is present, and are more sensitive to foundation deformation (even minor stress changes may cause concrete cracking). Due to the large scale of group piles, traditional on-site testing is time-consuming and labor-intensive, and model experiments are complex to operate. This study constructs numerical models with uniform and non-uniform sediment thicknesses to systematically analyze the influence mechanism of sediment thickness on the bearing characteristics of group piles.

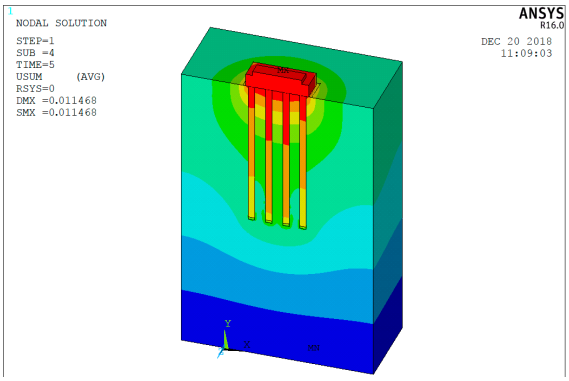
After the modeling is completed, a certain amount of uniform load is applied to the top of the pile cap, and the nonlinear solution can be carried out. After the calculation is finished, the calculation results are viewed, as shown in Figure 15, which is the model displacement cloud diagram when a 1.5 MPa uniform load is applied.



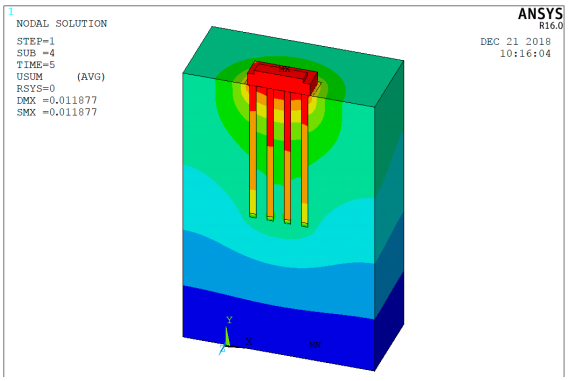
(**a**) No sediment model



(**b**) A 20 cm sediment model

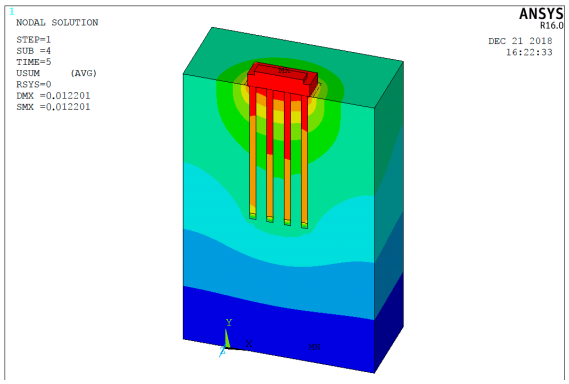


(**c**) Sediment model, 60 cm



(**d**) Sediment model, 100 cm

Figure 15. *Cont*.



(**e**) Model of sediment, 140 cm

Figure 15. Displacement cloud of the group pile model.

As can be seen from Figure 15 above, the change in sediment thickness affects the displacement distribution law and maximum settlement value of the model, which will be analyzed in detail in the next section.

3.3. Bearing Characteristics of Group Pile Foundation Under Uniform Sediment Thickness

The load and maximum settlement of each model are extracted to make the load–settlement curve, as shown in Figure 16.

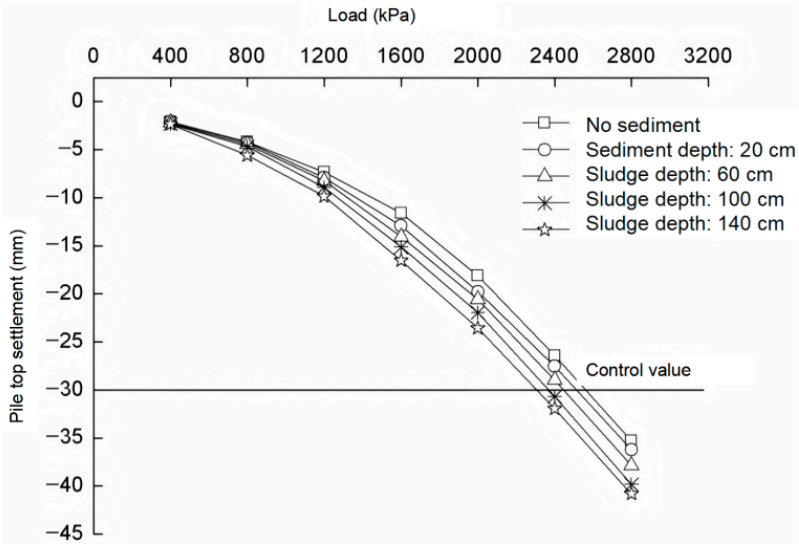


Figure 16. Load–sediment curve of the group pile model.

As shown in Figure 16, the maximum settlement of the group pile foundation occurs at the top of the cap. The settlement values of individual piles vary, and along the driving direction, the left and right piles exhibit symmetrical settlement patterns. The central pile shows greater settlement than the side piles. Within the same horizontal plane, the settlement of the pile foundation exceeds that of the surrounding soft-rock mass. All load–settlement curves follow a parabolic pattern. Under identical loading conditions, settlement increases with accumulated sediment thickness. By defining the load corresponding to 30mm settlement on the curve as the ultimate bearing capacity of the group pile foundation, we obtain its limits for each sediment thickness, as detailed in Table 6.

Table 6. Limit of bearing capacity of each group pile model.

Order Number	Pile Sedimentation Thickness (cm)	Sediment Thickness/Diameter of Pile	Limits of Group Pile Bearing Capacity (kN)	Discount Coefficient
1	0	\	173,945.0	\
2	20	0.133	169,987.8	0.977
3	60	0.400	166,092.7	0.955
4	100	0.667	161,015.7	0.926
5	140	0.933	156,187.2	0.898

Compared with the pile, the sediment thickness has a small influence on the settlement and ultimate bearing capacity of the group pile. This is because the bearing platform and soft-rock mass under the group pile foundation also play a role in bearing, which weakens the influence of sediment on the settlement of the group pile. It shows that the low-bearing platform group pile can greatly overcome the influence of sediment on the pile foundation.

As can be seen from the previous section, the settlement law of each pile foundation is not completely the same. Therefore, this section extracts the settlement cloud diagram of the pile foundation under normal bearing load, that is, 1.5MPa uniform load, as shown in Figure 17, to analyze the settlement deformation distribution law of the pile foundation.

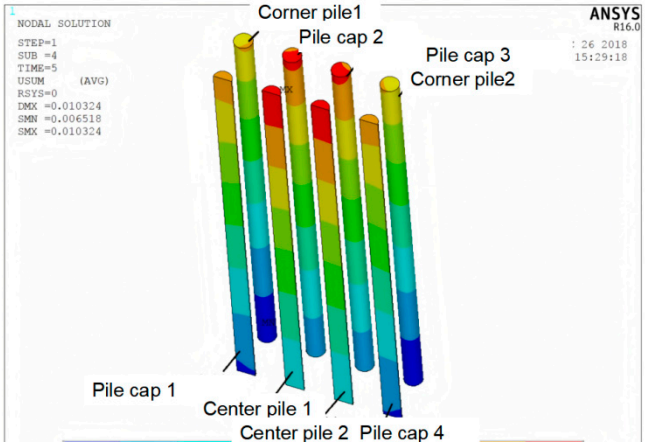


Figure 17. Cloud diagram of pile settlement in the non-sediment model.

Figure 17 shows that in the specific loading conditions of the group pile model, the top settlement of each pile is the greatest, gradually decreasing along the pile body, and the bottom settlement is the smallest. The settlement pattern is central pile > side pile > corner pile, and it is symmetrically distributed along the longitudinal axis of the bridge. It is worth noting that the top settlement of the corner piles (such as corner pile 1) and the side piles (side piles 2 and 3) on the side closer to the center of the bridge pier cap is significantly greater than that on the opposite side. This uneven settlement may cause stress concentration, leading to concrete cracking and endangering the stability of the connection between the pile and the bridge pier cap. The numerical model further indicates that under the same ultimate bearing capacity (2.4 MPa), there is a nonlinear relationship between the pile-top settlement and the deposition thickness (see Figure 13), and different positions of the piles exhibit different settlement characteristics due to the difference in deposition thickness.

As shown in Figure 18, the pile-top settlement under the same cap load gradually increases with increasing sediment thickness. The settlement values for different sediment thicknesses follow this pattern: central pile 1 > side pile 2 > side pile

1 > corner pile 1. When sediment thickness ranges from 0 to 140 cm, central pile 1 shows a 30.5% increase in settlement, side pile 2 a 29.7%, side pile 1 a 30.1%, and corner pile 1 a 27.3%. The order of settlement influence on pile tops by sediment thickness is central pile 1 > side pile 1 > side pile 2 > corner pile 1. Therefore, central piles are most affected by sediment, requiring special attention during preliminary design or actual construction.

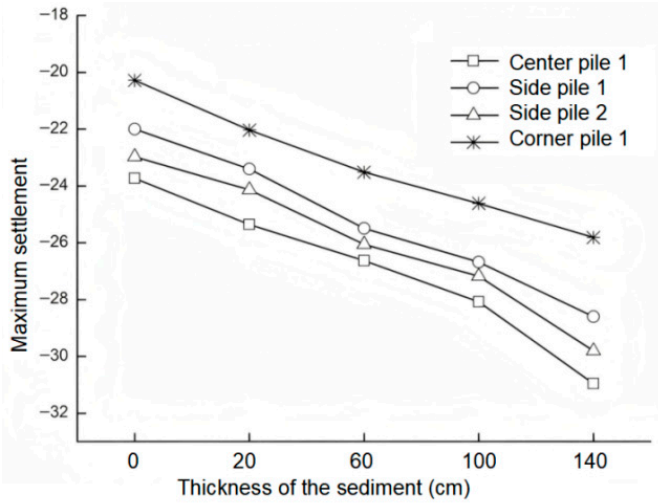


Figure 18. Relationship between maximum settlement of pile foundation and sediment thickness.

3.4. Analysis of Seismic Load Acting on the Bridge

The unsteady sediment numerical model along the longitudinal direction of the bridge was simplified into a two-dimensional model, as shown in Figure 19. The foundation pile has a diameter of 1.5 m, length of 34.5 m, and spacing of 4 m. Contact zones were established at the base of the cap, pile sides, and the interface between pile bases and soft-rock mass. The displacement cloud diagram for the non-sediment model is shown in Figure 20, while the displacement cloud diagram for the 1 m sediment thickness model is presented in Figure 21, with corresponding stress cloud diagrams in Figure 22. The seismic load effects along the longitudinal direction of the bridge are detailed in Table 7.

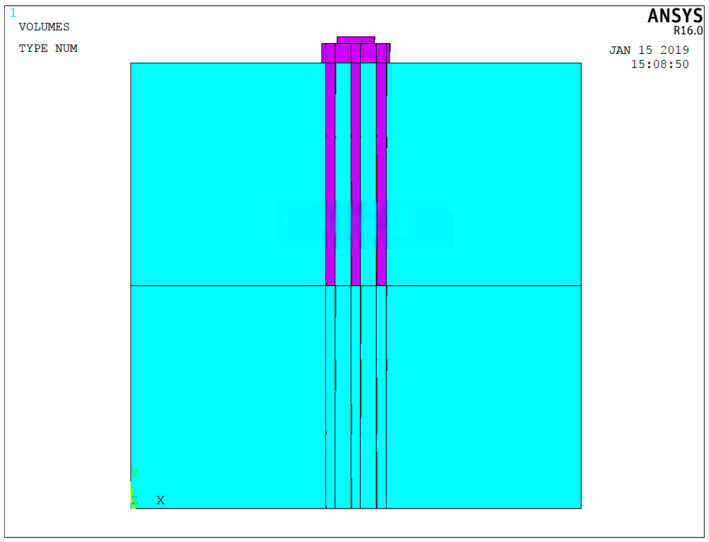


Figure 19. Numerical model of group pile in direction of bridge.

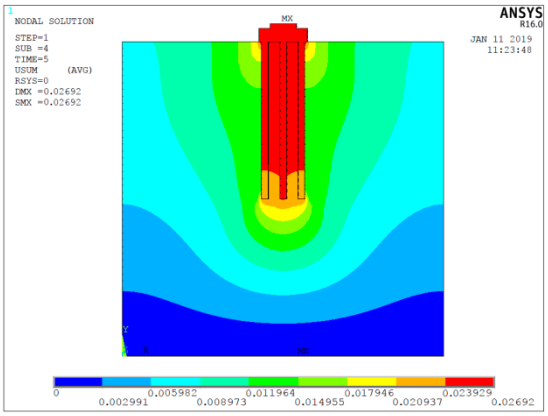


Figure 20. Displacement cloud of the sediment-free model.

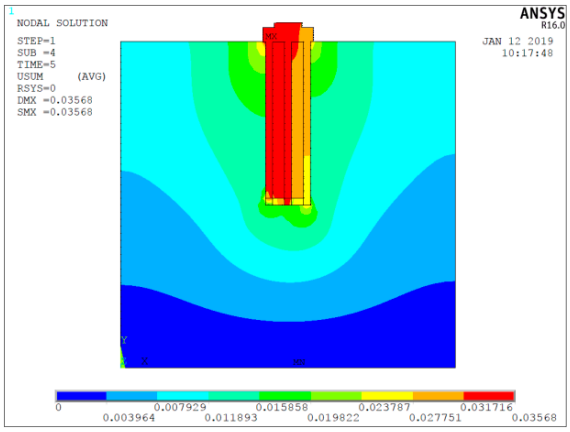


Figure 21. Displacement cloud of the sediment thickness.

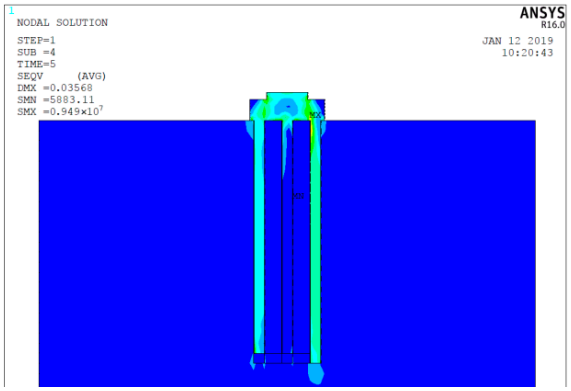


Figure 22. Stress cloud of the sediment thickness.

As shown in Table 7, under seismic loads along the bridge direction, pile 1 (with sediment) exhibits significantly increased settlement as seismic acceleration intensifies. According to the "Seismic Design Code for Buildings", horizontal seismic influence coefficients must be considered when evaluating seismic effects, with values ranging from 0.1 g to 10 g corresponding to different intensity zones. The sediment in pile 1 reduces its bearing capacity, causing greater settlement during earthquakes and creating a "sediment–seismic" dual effect. The stress concentration point shifts to the top of pile 3 (a sediment-free pile), aligning with the principle that "sediment-free piles bear greater loads".

Table 7. Characteristics of the bridge under seismic load in the direction of the bridge.

Seismic Acceleration	Maximum Settlement Value (mm)	Deposition Growth Rate	Maximum Stress Value (MPa)	Stress Growth
No seismic load	26.92	-	5.83	-
0.1 m/s^2	28.20	4.75%	6.20	6.35%
0.5 m/s^2	30.15	12.00%	7.15	22.64%
1.0 m/s^2	32.40	20.36%	8.00	37.22%
5.0 m/s^2	38.50	43.01%	10.50	80.10%
10 m/s^2	45.00	67.16%	13.00	123.16%

3.5. Analysis of Seismic Load Acting on Transverse Bridge

Statistical analysis of transverse seismic loads is shown in Figure 23. The displacement cloud diagram for the 1 m sediment thickness model is presented in Figure 24, while the stress cloud diagram for the same model is illustrated in Figure 25. The bridge characteristics under transverse seismic loads are detailed in Table 8.

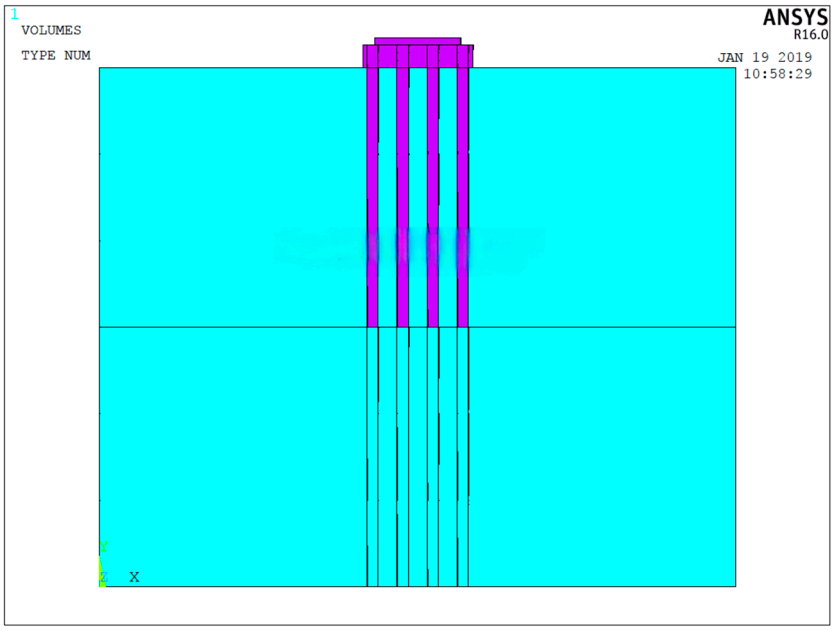


Figure 23. Numerical model of transverse bridge to group pile.

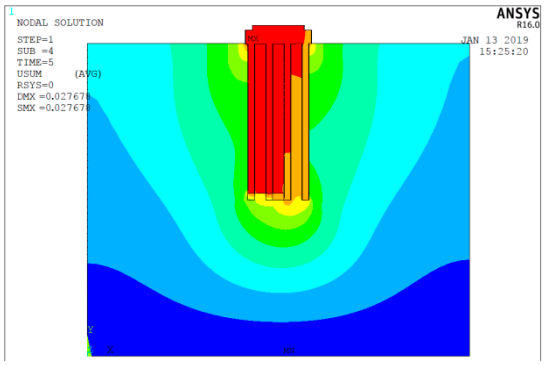


Figure 24. Displacement cloud of the 1 m sediment thickness model.

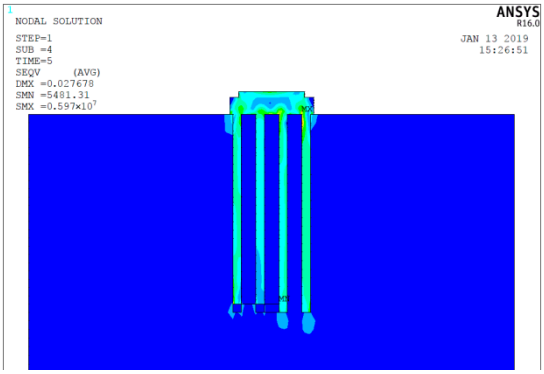


Figure 25. Stress cloud of the 1 m sediment thickness model.

Table 8. Bridge characteristics under seismic load of transverse bridge.

Seismic Acceleration	Maximum Settlement Value (mm)	Deposition Growth Rate	Maximum Stress Value (MPa)	Stress Growth	Most Unfavorable Working Condition Characteristics
No seismic load	24.79	-	4.95	-	No sediment reference
0.1 m/s^2	26.00	4.88%	5.20	5.05%	Slight inclination of piles
0.5 m/s^2	28.00	12.95%	5.80	17.17%	Pile 2 settles obviously
1.0 m/s^2	30.50	23.03%	6.50	31.31%	Pile tilting intensifies
5.0 m/s^2	35.00	41.17%	8.00	61.62%	Pile 2 severe settlement
10 m/s^2	40.00	61.34%	10.00	102.02%	Overall instability of pile group

Seismic loads caused by transverse bridge vibrations induced a "twisting–inclining" composite effect in the pile group. Condition 6 (with sediment in piles 1, 3, and 4, but no sediment in pile 2) became the most unfavorable scenario, as pile 2 (the non-sediment-bearing pile) had to bear greater horizontal loads, resulting in peak stress concentration at its tip reaching 6.41 MPa (10 m/s^2). Research on dynamic responses of pile groups under seismic loading revealed that the front-row pile (pile 2) exhibited maximum horizontal bearing capacity, while the rear-row pile's capacity decreased due to edge effects, forming a "compressive front, tensile rear" stress distribution pattern.

The influence of sediment thickness stems from static load-bearing mechanisms, where reduced pile-end resistance leads to increased settlement. Seismic loads, however, represent dynamic effects amplified by inertial forces and soil–pile interactions that intensify displacement and stress.

4. Theoretical Analysis of Seismic Bearing Capacity of Pile Foundation Under Different Working Conditions

4.1. Theoretical Model and Formula Derivation

Based on the above theory, we established a model to investigate the influence of sediment under earthquake action on the bearing characteristics of the group pile foundation, which is derived by the following formula:

Pile-end bearing capacity correction coefficient:

$$K_p = 1 - \beta \tag{1}$$

where K_p is the bearing capacity correction coefficient of the pile end, and β is the sediment influence coefficient.

Side friction resistance correction coefficient of pile:

$$K_s = 1 - \beta \mathrm{h} \tag{2}$$

where h is the sediment thickness.

Combined with Formulas (1) and (2), the revised total bearing capacity:

$$Q'_{total} = Q_p K_p + Q_s \mathrm{K_s} \tag{3}$$

Earthquake power amplification coefficient:

$$DAF = 1 + \frac{PGA}{g} \tag{4}$$

PGA is the peak ground acceleration, and g is the gravitational acceleration

Combined with Formula (4), equivalent carrying capacity:

$$Q_{eq} = Q'_{total} DAF \tag{5}$$

Combined with Formulas (1) and (5), safety factor:

$$FS = \frac{Q_{eq}}{Q_{design}} \tag{6}$$

Qdesign is the design load

Pile-end bearing capacity:

$$Q_p = A_p \, \sigma_0 \tag{7}$$

Side friction resistance of pile:

$$Q_s = \pi D L \tau \tag{8}$$

Pile-end area:

$$A_p = \frac{\pi D^2}{4} \tag{9}$$

Rapidity of bearing capacity change:

$$\frac{dQ_{eq}}{dPGA} = Q'_{total} \tag{10}$$

Combined with Formula (5), the derivative of sediment thickness to bearing capacity:

$$\frac{dQ_{eq}}{d\mathrm{h}} = -\beta Q'_{total} DAF \tag{11}$$

Combined with Formula (11), the second-order differential equation of bearing capacity:

$$\frac{d^2 Q_{eq}}{dPGA^2} = 0 \tag{12}$$

Laplace transform of bearing capacity:

$$L\{Q_{eq}\} = \int_0^{\infty} e^{-st} Q_{eq}(t)dt \tag{13}$$

The Fourier transform of load-bearing capacity:

$$F\{Q_{eq}\} = \int_{-\infty}^{\infty} e^{-i\omega t} Q_{eq}(t)dt \tag{14}$$

Combined with Formulas (13) and (14), the bearing capacity correction coefficients considering sediment and earthquake are considered:

$$\lambda = \frac{Q_{eq}}{Q_0} = 1\beta\mathrm{h} + DAF\beta\mathrm{h}DAF \tag{15}$$

Differential equation of pile foundation bearing capacity:

$$\frac{dQ_{eq}}{dPGA} = Q'_{total}(1 - \beta\mathrm{h}) \tag{16}$$

Rate of change in sediment thickness:

$$\frac{d\mathrm{h}}{dPGA} = kPGA \tag{17}$$

Combined with Formulas (16) and (27), bearing capacity sensitivity to sediment thickness:

$$S_{\mathrm{h}} = \frac{dQ_{eq}}{d\mathrm{h}} = -\beta Q'_{total}DAF \tag{18}$$

Sensitivity of bearing capacity to seismic intensity:

$$S_{PGA} = \frac{dQ_{eq}}{dPGA} = Q'_{total}(1 - \beta\mathrm{h}) \tag{19}$$

The secondary relationship between bearing capacity and seismic intensity:

$$Q_{eq} = Q_0(1 + PGA) - \beta\mathrm{h}Q_0(1 + PGA) \tag{20}$$

Combined with Formula (20), the secondary relationship between bearing capacity and sediment thickness:

$$Q_{eq} = Q_0(1 - \beta\mathrm{h}) + Q_0(1 - \beta\mathrm{h})PGA \tag{21}$$

Combined with Formula (21), the Taylor series expansion of bearing capacity:

$$Q_{eq} = Q_0 + Q_0PGA - \beta Q_0\mathrm{h} - \beta Q_0\mathrm{h}PGA \tag{22}$$

Combined with Formulas (20) and (22), the logarithmic relationship of bearing capacity:

$$\ln Q_{eq} = \ln Q_0 + \ln(1 + PGA) + \ln(1\beta\mathrm{h}) \tag{23}$$

Index relationship of bearing capacity:

$$Q_{eq} = Q_0 e^{PGA}(1 - \beta\mathrm{h}) \tag{24}$$

Integral form of bearing capacity:

$$Q_{eq} = \int_0^{PGA} Q'_{total}(1 - \beta h)dPGA \tag{25}$$

Combined with Formulas (15) and (25), the differential equation group of bearing capacity:

$$\frac{dQ_{eq}}{dPGA} = Q'_{total}(1\beta h) \tag{26}$$

$$\frac{dh}{dPGA} = kPGA \tag{27}$$

Combined with Formula (26), the Laplace transform solution of bearing capacity:

$$L\{Q_{eq}\} = \frac{Q_0(1-\beta h)}{s} + \frac{Q_0(1-\beta h)}{s^2} \tag{28}$$

Fourier transform solution of bearing capacity:

$$F\{Q_{eq}\} = \frac{Q_0(1-\beta h)}{i\omega} + \frac{Q_0(1-\beta h)}{(i\omega)^2} \tag{29}$$

Combined with Formulas (6) and (29), the optimization expression of the safety factor:

$$FS = \frac{Q_{eq}}{Q_{design}} = \frac{Q_0(1 - \beta h)(1 + PGA)}{Q_{design}} \tag{30}$$

4.2. Analysis of Bearing Capacity Variation Law Under Different Working Conditions

Based on the above theoretical formula, we calculated and analyzed the bearing capacity of pile foundations under different combinations of seismic intensity (PGA) and sediment thickness (h). Table 9 shows the variation in bearing capacity of pile foundations under different combinations of seismic intensity and sediment thickness

The seismic intensity (PGA) is significantly positively correlated with the safety factor (FS): when PGA increases from 0.1 g to 10 g, FS rises from 1.209 to 37.654 (an increase of 2930.4%), with an average increase of approximately 1.8 for every 0.1 g increase. This relationship is mainly driven by the dynamic amplification effect (DAF = 1 + PGA), the seismic design adjustment coefficient (E1 = 1.5), and the safety factor calculation formula (FS = Qeq/Q design).

The thickness of sediment (h) is significantly negatively correlated with FS: when h increases from 0.05 m to 0.20 m, FS decreases from 2.510 to 1.209 (a decrease of 51.9%), with an average decrease of 0.32 for every 0.05 m increase. This is because the supporting capacity of the sediment layer decreases as the thickness increases (the bearing capacity correction coefficient of the pile tip/side Kp/Ks = 1 − βh decreases), and the high water content of the soft-rock area sediment is prone to liquefaction, further weakening the bearing capacity of the pile foundation.

The coupling effect between earthquake intensity and sediment thickness is very significant. The phenomenon of a reduction of approximately 1.5% in the safety factor as the sediment thickness increases has been confirmed. This indicates that under high earthquake intensity, the negative impact of sediment thickness on the safety factor is relatively stable. In low-earthquake-intensity areas, the influence of sediment thickness on the safety factor is more significant. However, in high-earthquake-intensity areas, even with a large accumulation of sediment, the safety factor may still meet the specification requirements.

Table 9. Variation in bearing capacity of pile foundation under different seismic intensity and sediment thickness combinations.

Seismic Intensity (PGA, g)	Sediment Thickness (h, m)	Pile-End Bearing Capacity (kN)	Side Friction Resistance of Pile (kN)	Total Bearing Capacity (kN)	Equivalent Carrying Capacity (kN)	Safety Factor (FS) Calculated	Code Requirements (FS $\geq$ 2.5)
0.1	0.05	497.5	4477.5	4975.0	5472.5	1.227	dissatisfaction
0.1	0.10	495.0	4455.0	4950.0	5445.0	1.221	dissatisfaction
0.1	0.15	492.5	4432.5	4925.0	5417.5	1.215	dissatisfaction
0.1	0.20	490.0	4410.0	4900.0	5390.0	1.209	dissatisfaction
0.5	0.05	497.5	4477.5	4975.0	11,193.75	2.510	satisfied
0.5	0.10	495.0	4455.0	4950.0	11,137.50	2.498	dissatisfaction
0.5	0.15	492.5	4432.5	4925.0	11,081.25	2.485	dissatisfaction
0.5	0.20	490.0	4410.0	4900.0	11,025.00	2.472	dissatisfaction
1.0	0.05	497.5	4477.5	4975.0	16,790.63	3.765	satisfied
1.0	0.10	495.0	4455.0	4950.0	16,706.25	3.747	satisfied
1.0	0.15	492.5	4432.5	4925.0	16,621.88	3.728	satisfied
1.0	0.20	490.0	4410.0	4900.0	16,537.50	3.709	satisfied
5.0	0.05	497.5	4477.5	4975.0	83,953.13	18.827	satisfied
5.0	0.10	495.0	4455.0	4950.0	83,531.25	18.733	satisfied
5.0	0.15	492.5	4432.5	4925.0	83,109.38	18.638	satisfied
5.0	0.20	490.0	4410.0	4900.0	82,687.50	18.543	satisfied
10.0	0.05	497.5	4477.5	4975.0	167,906.25	37.654	satisfied
10.0	0.10	495.0	4455.0	4950.0	167,062.50	37.466	satisfied
10.0	0.15	492.5	4432.5	4925.0	166,218.75	37.277	satisfied
10.0	0.20	490.0	4410.0	4900.0	165,375.00	37.089	satisfied

The data in Table 9 shows that 7 out of 20 seismic conditions (35%) meet the code requirements (FS $\geq$ 2.5), while 13 (65%) do not. The compliant conditions mainly include PGA $\geq$ 0.5 g and h = 0.05 m conditions (1) and all PGA $\geq$ 1.0 g conditions (12). The non-compliant conditions primarily consist of all PGA = 0.1 g conditions (4) and PGA = 0.5 g conditions with h $\geq$ 0.10 m (3). Although a seismic intensity of 0.5 g serves as the critical threshold for meeting safety factors in code compliance, it must be combined with sediment thickness control (h $\leq$ 0.05 m). Therefore, in low-seismic-intensity areas (PGA < 0.5 g), sediment thickness should be strictly controlled within 0.05 m; in high-seismic-intensity areas (PGA $\geq$ 1.0 g), sediment thickness may be appropriately increased to 0.20 m while still meeting code safety factor requirements.

5. Conclusions

This study conducted experiments and simulation analyses to investigate the mechanical responses of bridge foundation piles and sediments under seismic action. The results show that seismic forces have a significant nonlinear impact on the bearing capacity of embedded sand layer piles: when the PGA increases from 0 to 10 m/s^2, the decline rate of bearing capacity rises from 0% to 55.3%, and the settlement increases from 3.2 mm to 18.5 mm (an increase of 478%). When the PGA is $\geq$0.2 m/s^2, the sand layer cohesion failure leads to semi-liquefaction; when $\geq$1.0 m/s^2, complete liquefaction occurs, and the resistance loss reaches 80%. The seismic motion causes an increase in pore water pressure. When PGA > 5 m/s^2, the shear modulus of the sand layer drops to less than 15% of the original value, accelerating the growth of settlement.

The thickness of the sediment has a strong linear relationship with the reduction rate (R^2 = 0.98): when the thickness is greater than 0.8 cm, it enters the "danger zone" (reduction rate > 30%), and for every 0.1 cm increase in thickness, the reduction rate increases by 4.7%.

The liquefaction risk of fine-grained sediment (<0.1 mm) is significantly higher than that of coarse-grained sediment (>0.2 mm). For every 1.0 cm increase in fine-grained sediment thickness, the reduction rate decreases by 9.8%, which is much higher than the 3.6% for coarse-grained sediment.

Under the longitudinal seismic load of the pile group, the settlement growth rate of the sediment-containing piles reaches 67.16%, triggering the "sediment–seismic" dual effect; the lateral load leads to the "torsional inclination" composite effect, and the stress at the top of the non-sediment piles reaches 6.41 MPa. Under the combined effect, the settlement growth rate is 99.7%, the stress growth rate is 185.94%, presenting a superimposed failure mode. The safety factor (FS) is strongly positively correlated with PGA, while being negatively correlated with the sediment thickness (h). This study provides key parameters and optimization basis for bridge design in high-intensity seismic zones. Future research is needed to deepen the study of the long-term performance evolution of sediments and the multi-factor synergy effect, and to improve the seismic reliability of pile foundations in soft-rock areas.

Author Contributions: Conceptualization, X.Y., X.M., H.W. and H.C., methodology; software, H.W. and H.C.; writing—original draft preparation, X.Y.; writing—review and editing, X.Y.; project administration, X.M.; funding acquisition, X.M. All authors have read and agreed to the published version of the manuscript.

Funding: This work was supported in part by the Science and Technology Research Project of Henan Province under Grant 242102241014 and in part by the Key Scientific Research Projects of Colleges and Universities in Henan Province under the Grant No. 24B560029.This study was supported by the Xuchang City Key R&D and Promotion Special Project (Grant Number 20230211016).This study was supported by New Round Key Discipline of Civil and Hydraulic Engineering of Henan, China (grant no. 2023414349) and Program for Innovative Research Team at Zhongyuan Institute of Science and Technology (grant no. ZYKJCXTD202402), and the National Natural Science Foundation of China (Grant No. 52308393) and the State Key Laboratory of Precision Blasting and Hubei Key Laboratory of Blasting Engineering, Jianghan University (Grant No. PBSKL2023B2).

Data Availability Statement: The data in this study are presented in the full manuscript.

Conflicts of Interest: The authors declare no conflicts of interest.

References

1. Yang, Y.; Zhang, P.; Wu, L.; Zhang, Q. Study on the Influence of Water Erosion on the Bearing Capacity and Function of the High Pile Foundation of the Wharf. *Water* **2024**, *16*, 606. [CrossRef]
2. Zhu, W.; Cheng, J.; Pang, Y.; An, H.; Zou, J.; Ren, J.; Zhang, C. Quasi-Static Test and Lateral Load-Bearing Capacity of a New Grid Pile Foundation for Long-Span Bridges. *Appl. Sci.* **2024**, *14*, 1209. [CrossRef]
3. Qian, Y.; Li, Y.; Li, X.; Wang, Z.; Yang, Y.; Teng, D.; Ma, Z. Influence of bearing platform size on bearing capacity of NT-CEP pile group foundation under compound force. *Sci. Rep.* **2025**, *15*, 10753. [CrossRef] [PubMed]
4. Zou, X.; Yang, Z.; Hu, J. Bearing capacity of monopile-bucket composite foundation in sand-over-clay under V-H-M combined static loads. *Appl. Ocean Res.* **2024**, *150*, 104092. [CrossRef]
5. Sheng, M.; Lu, F.; Jiang, N.; Guo, P.; Li, X.; An, R.; Wang, Y. Bearing behavior of pile foundation in karst region: Physical model test and finite element analysis. *Appl. Rheol.* **2024**, *34*, 20230115. [CrossRef]
6. Cao, Y.; Ni, J.; Chen, J.; Geng, Y. Rapid Evaluation Method to Vertical Bearing Capacity of Pile Group Foundation Based on Machine Learning. *Sensors* **2025**, *25*, 1214. [CrossRef]
7. Chen, G.; Gu, H.; Liu, R.; Li, T.; Liang, C. Upper bound solution of the vertical bearing capacity of the pile-bucket composite foundation of offshore wind turbines. *Mar. Struct.* **2025**, *100*, 103728. [CrossRef]
8. Mittal, V.; Samanta, M. Influence of Spacing and Slenderness Ratio of End-Socketed Pile Foundation on Seismic Response of Building Considering Soil–Pile–Structure Interaction: An Experimental Approach. *J. Struct. Eng.* **2025**, *151*, 04024213. [CrossRef]
9. Shen, K.; Zhang, H.; Liu, J.; Zhao, X.; Zhang, Y. Study of cement-soil mixed piles reinforcement method for offshore wind turbine pile foundation. *Ocean Eng.* **2024**, *313*, 119423. [CrossRef]

10. Ma, P.; Deng, Z.; Zhang, S.; Zhang, Y.; Huang, Y.; Yuan, C. Investigation of engineering-scale testing and bearing capacity calculation method for rotary screw special-shaped piles. *Can. Geotech. J.* **2025**, *62*, 1–16. [CrossRef]
11. Chen, S.; Zou, X.; Tu, X.; Liang, C. Effects of local scouring on capacities of monopile-wheel composite foundations in sand under lateral loading. *Mar. Georesources Geotechnol.* **2024**, *42*, 1543–1559. [CrossRef]
12. Zhang, M.; Yang, J.; Yang, Y.; Xu, D.-S.; Zhou, Y.-S. Study on Load Bearing Characteristics of Novel Expandable Deepwater Drilling Conductor Based on Laboratory Experiment and Field Test. *China Ocean Eng.* **2023**, *37*, 16–28. [CrossRef]
13. Wei, J. Bearing Characteristics and Negative Skin Friction Preventive Measures for Highway Bridge Pile Foundations in Collapsible Loess Areas Under Water Immersion. *Water* **2024**, *16*, 3587. [CrossRef]
14. Wang, L.; Zhao, Q.; Wu, J. Numerical study on the group wall effect of nodular diaphragm wall foundation in high-rise buildings. *Open Geosci.* **2023**, *15*, 20220562. [CrossRef]
15. Lee, H.; Choi, M.K.; Kim, B.J. Feasibility of concrete-filled fiber-reinforced plastic piles for deep foundation: A comprehensive review on geotechnical and structural characteristics. *Carbon Lett.* **2024**, *34*, 315–329. [CrossRef]
16. Amiri, A.; Majdeddin, M.M.H.S.; Soroush, A. Experimental study of influencing pile to cap connections on the rocking behaviors of piled foundations. *Sci. Rep.* **2025**, *15*, 14937. [CrossRef]
17. Nguyen, T.Q.; Tu, V.B.; Nguyen, D.N. Enhancing water pressure sensing in challenging environments: A strain gage technology integrated with deep learning approach. *Meas. Control* **2025**, *58*, 208–226. [CrossRef]
18. Li, P.; Xia, Y.; Xie, X.; Wang, J.; Wang, C.; Shi, M.; Wang, B.; Wu, H. Study on Vertical Bearing Capacity of Pile Foundation with Distributed Geopolymer Post-Grouting on Pile Side. *Materials* **2024**, *17*, 398. [CrossRef]
19. Izumi, K.; Ogihara, M.; Kameya, H. Displacements of bridge foundations on sedimentary soft rock: A case study on small-strain stiffness. *Géotechnique* **1997**, *47*, 619–632. [CrossRef]
20. Islam, M.; Siddiquee, M.; Tatsuoka, F. A nonlinear model for soft rock and its application in bridge pier settlement calculation. In Proceedings of the Japan-Bangladesh Joint Seminar on Advances in Bridge Engineering, Dhaka, Bangladesh, 21–22 August 2015; pp. 19–32.
21. Huang, B.; Wen, K. A New Type DSS Device and Its Application in Shaft Friction of Pile in Soft Rock. *Strength Mater.* **2024**, *56*, 1286–1296. [CrossRef]
22. Kroon, I.B.; Park, H.; Özener, A.; Mete, D.; Yamasaki, Y. 1915 Çanakkale Bridge–Detailed Design. *IABSE Rep.* **2023**, *119*, 552–559. [CrossRef]
23. Belzer, B.E.; Lingwall, B.N.; Roberts, L.A. A Review of LRFD Bridge Foundation Design and Construction in South Dakota. In Proceedings of the Geo-Congress 2020: University of Minnesota 68th Annual Geotechnical Engineering Conference (GSP 321), Minneapolis, MN, USA, 25–28 February 2020. [CrossRef]
24. Tran, D.; Ahmed, Z.; Nguyen, Q.B. Application of Plaxis for Calculating the Construction Stability and Soft Embankment in Protecting ha Thanh River, Binh Dinh Province. In Proceedings of the 2nd Conference on Sustainability in Civil Engineering (CSCE'20), Islamabad, Pakistan, 12 August 2020.
25. Mohammadi, S.D.; Mortezaei, R.; Sarfarazi, V.; Salehipor, P. Delay failure and fast fracturing of notched bedding rock under shear test condition: Physical test and discrete element simulation. *Comput. Part. Mech.* **2025**, *12*, 673–691. [CrossRef]
26. Mortezaei, R.; Mohammadi, S.D.; Sarfarazi, V.; Far, A.M. Investigation of shear behavior of notched bedding rock containing welded interface between hard and soft layers; an acoustic emission-based approach. *Theor. Appl. Fract. Mech.* **2023**, *127*, 23. [CrossRef]
27. Mohammadi, S.D.; Mortezaei, R.; Sarfarazi, V.; Abharian, S. Investigation of acoustic events during shear loading of layered rock bridge: Particle flow code approach. *Multiscale Multidiscip. Model. Exp. Des.* **2024**, *7*, 4657–4681. [CrossRef]
28. Joseph, A.; Anil, A.; Biju, S.S.; Pomson, S.S. Case Study on Embankment Failure of Bridge at Mahe–Thalassery Bypass, Kerala, India. In Proceedings of the International Conference on Transportation Geotechnics, Sydney, Australia, 20–22 November 2024; Springer: Singapore, 2025. [CrossRef]
29. Adebayo, B.; Ajaka, E.O.; Afeni, T.B.; Taiwo, B.O.; Okewale, I.A.; Lawal, A.I.; Ogunyemi, B.O.; Apena, W.O.; Akinbinu, V.A.; Amigun, J.O. Enhancing downstream operation through run-of-mine crusher selection model: An application of edge detection software and soft computing algorithms. *Arab. J. Geosci.* **2024**, *17*, 15–29. [CrossRef]

Disclaimer/Publisher's Note: The statements, opinions and data contained in all publications are solely those of the individual author(s) and contributor(s) and not of MDPI and/or the editor(s). MDPI and/or the editor(s) disclaim responsibility for any injury to people or property resulting from any ideas, methods, instructions or products referred to in the content.